An Integrated Microfluidic Device for Monitoring Changes in Nitric Oxide Production in Single T-Lymphocyte (Jurkat) Cells

Eve C. Metto,[†] Karsten Evans,[†] Patrick Barney,[†] Anne H. Culbertson,[†] Dulan B. Gunasekara,[‡,§] Giuseppe Caruso,[§,‖] Matthew K. Hulvey,[§,⊥,#] Jose Alberto Fracassi da Silva,[§,∞,○] Susan M. Lunte,[‡,§,⊥] and Christopher T. Culbertson*,[†]

[†]Department of Chemistry, Kansas State University, Manhattan, Kansas 66506, United States

[‡]Department of Chemistry, University of Kansas, Lawrence, Kansas 66045, United States

[§]Ralph N. Adams Institute for Bioanalytical Chemistry, University of Kansas, 2030 Becker Drive, Lawrence, Kansas 66047, United States

[‖]Department of Chemical Science, Section of Biochemistry and Molecular Biology, The University of Catania, I-95124 Catania, Italy

[⊥]Department of Pharmaceutical Chemistry, University of Kansas, Lawrence, Kansas 66047, United States

[#]Akermin, Inc., St. Louis, Missouri 63132, United States

[∞]Institute of Chemistry, State University of Campinas, São Paulo 13083-970, Brazil

[○]Instituto Nacional de Ciência e Tecnologia em Bioanalítica (INCTBio), Brazil

S *Supporting Information*

ABSTRACT: A considerable amount of attention has been focused on the analysis of single cells in an effort to better understand cell heterogeneity in cancer and neurodegenerative diseases. Although microfluidic devices have several advantages for single cell analysis, few papers have actually demonstrated the ability of these devices to monitor chemical changes in perturbed biological systems. In this paper, a new microfluidic channel manifold is described that integrates cell transport, lysis, injection, electrophoretic separation, and fluorescence detection into a single device, making it possible to analyze individual cells at a rate of 10 cells/min in an automated fashion. The system was employed to measure nitric oxide (NO) production in single T-lymphocytes (Jurkat cells) using a fluorescent marker, 4-amino-5-methylamino-2′,7′-difluorofluorescein diacetate (DAF-FM DA). The cells were also labeled with 6-carboxyfluorescein diacetate (6-CFDA) as an internal standard. The NO production by control cells was compared to that of cells stimulated using lipopolysaccharide (LPS), which is known to cause the expression of inducible nitric oxide synthase (iNOS) in immune-type cells. Statistical analysis of the resulting electropherograms from a population of cells indicated a 2-fold increase in NO production in the induced cells. These results compare nicely to a recently published bulk cell analysis of NO.
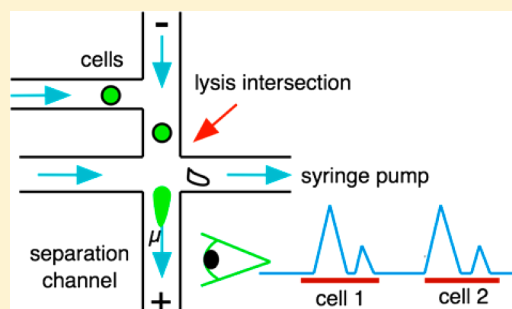
The biochemical heterogeneity displayed by seemingly identical cells is known to play an important role in many diseases, including cancer, neurodegenerative disorders, and cardiovascular diseases.[1] Chemical analysis of individual cells can be used to probe this heterogeneity and identify biochemical variations in a population of cells.[1,2] For example, immune cells exhibit such biological heterogeneity in terms of the extent of their expression of the inducible form of nitric oxide synthase (iNOS) in response to infection and inflammation.[3−5] While nitric oxide (NO) is generated by various forms of NOS, changes in NO production in immune cells are generally controlled by changes in iNOS expression. NO is an important signaling molecule that is involved in a number of physiological processes, including blood pressure regulation,[6] neurotransmission, and the immune response.[7−9] NO production has been measured previously at the population level in immune cells by our groups,[10] in single neurons by the Sweedler group using capillary electrophoresis with laser-induced fluorescence[11−16] and in endothelial cells by Martin and Spence groups using microfluidic devices with electrochemical and fluorescence detection.[17−20] Immune cell types such as monocyte-derived macrophages and microglia are also known to exhibit phenotypes that have different levels of iNOS expression. These cell types are involved in the progression and prevention of cardiovascular and neurodegenerative diseases.[21−23] Therefore, a method that would enable the measurement of NO production in single immune cells as a
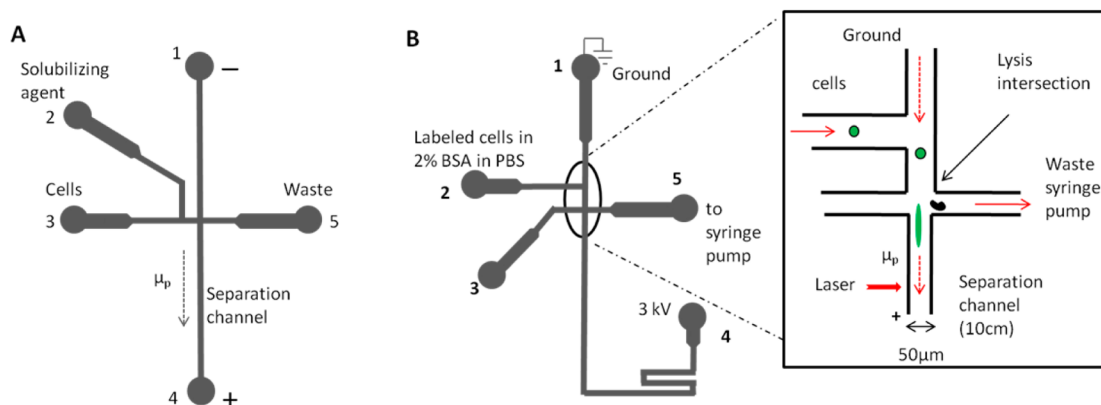
Figure 1. (A) Initial chip design and (B) schematic of improved microfluidic chip used for single cell lysis experiments. The lysis intersection of the microchip is shown in the inset. The solid arrows indicate the direction of bulk fluid flow, while the broken arrows show the direction of electrophoretic migration (μ_p).

function of different stimulants may aid in our understanding of the immune response and the progression of these diseases.

Many different methods such as flow cytometry, single cell imaging, liquid chromatography, capillary and microchip electrophoresis (ME), and microfluidic single cell cytometry have been developed to probe cellular heterogeneity. In the case of in vivo imaging and flow cytometry, it is not possible to resolve species that have same emission wavelengths, e.g., when multiple species react with the same fluorescent reporter molecule. In cases such as these, analytes cannot be differentiated from one another or concomitants.

To increase the number of species that can be analyzed, electrophoretic separation techniques have been developed for the analysis of single cells. Detection is most often accomplished using fluorescence, electrochemical, and mass spectrometric methods.[24−32] Conventional capillary electrophoresis methods, however, generally suffer from a low throughput because of difficulty in automating the injection of the cells and the fact that separations frequently take several minutes. This usually leads to a throughput on the order of less than a dozen cells per day,[29,33] although recently an exception to this was reported by the Allbritton group in which they described an automated capillary electrophoresis system for single cell analysis that showed significantly higher throughput (3.5 cells/min) than previous designs.[34] Another drawback of using capillaries for single cell analysis is that cell debris can adhere to the capillary wall, leading to irreproducibility in migration time and/or peak height/area and blockage of the lumen.[35]

The use of microfluidic-based devices has several potential advantages over capillary-based single cell analysis techniques. These include faster analysis times and thus higher throughput and smaller sample volume requirements that offer improved detection limits. Microfluidic devices are also more amenable to automation because it is possible to integrate several analytical procedures such as cell transport, cell lysis, and sample injection onto a single platform with better and more precise fluid control.[24,33,36−41] Separation-based microfluidic devices for single cell analysis provide the ability to determine a much larger number of analytes than is possible with many of the other approaches such as imaging and cytometry. With microchip electrophoresis, it is possible to separate several different analytes electrophoretically following cell lysis prior to detection. Most microchip electrophoresis (ME)-based single cell analysis experiments reported thus far have been proof-of-

principle studies on a small number of cells using test analytes,[24,42] although in a few cases, endogenous molecules[43−46] have also been measured. Only a couple of devices have been reported that have detected either test analytes[26] or endogenous molecules[47] in more than 100 cells per experiment.

In this paper, we report a high throughput microfluidic device designed for single cell analysis capable of analyzing 200 cells in 20 min (10 cells/min). These devices were modeled on an earlier etched glass design used in our lab and by others.[24,26,42,48] The device consists of a hybrid PDMS−glass chip that is easier to fabricate than previous all-glass designs. The geometry of the lysis and injection intersection have been modified to significantly improve the reproducibility of the lysate injection process. The device is employed to investigate the expression of iNOS by native and stimulated lymphocytes through the measurement of intracellular NO concentration. This is the first example of a microfluidic device being used with ME to serially measure intracellular NO in response to an external stimulation in over 100 individual cells in less than 10 min. The results of the single cell analysis experiments were compared to recently published bulk cell studies performed for the analysis of NO under identical stimulation conditions with good correlation.[10]

◼ EXPERIMENTAL SECTION

Reagents and Materials. Sodium borate, lyophilized bovine serum albumin (BSA), Tween-20, and acetonitrile (HPLC grade) were all obtained from Fisher Scientific (Pittsburgh, PA). Sodium dodecyl sulfate and anhydrous dimethyl sulfoxide, 99.9% (DMSO), were supplied by Sigma-Aldrich (St. Louis, MO). 4-Amino-5-methylamino-2′,7′-difluorofluorescein diacetate (DAF-FM DA) was obtained from Invitrogen Corporation, Carlsbad, CA, in 50 μg packs. 6-Carboxyfluorescein diacetate, 6-CFDA, was obtained from Fisher Scientific, Pittsburgh, PA. SU-8 2010 was purchased from MicroChem Corp. (Newton, MA). The SU-8 developer, 2-(1-methoxy)propyl acetate (99%), was obtained from Acros (Morris Plains, NJ). Silicon wafers, 4 in. in diameter, were purchased from Silicon, Inc. (Boise, ID). Sylgard 184 PDMS prepolymer and curing agent were purchased from Dow Corning (Corning, Inc., Corning, NY). Ultrapure water was generated from a Barnstead E-pure system (Dubuque, IA).

Microchip Fabrication. The microfluidic device (Figure 1) was fabricated using established soft lithography procedures.[49]

Briefly, SU-8 2010 negative photoresist was spun to a thickness of ~20 μm on a 4 in silicon wafer using a spin coater (Laurell Technologies Corp., North Wales, PA). The coated mask was then placed on a 65 °C hot plate for a 2 min soft bake followed by a 4 min hard bake on a 95 °C hot plate. A mask containing the microfluidic channel pattern, created using AutoCAD LT 2006 (Autodesk, San Rafael, CA), was placed on the wafer that was then exposed to ultraviolet light (ThermoOriel, Stratford, CT). The unpolymerized photoresist was washed off using SU-8 developer, rinsed with isopropyl alcohol, and blown dry with nitrogen. A 10:1 w/w mixture of PDMS prepolymer and curing agent was then poured over the mold and cured for at least 50 min at 80 °C. Access holes to the channels were drilled on a 75 mm × 50 mm glass slide (Corning, Inc.) using a 2 mm diamond-tipped drill bit (Rio Grande, Albuquerque, NM) and fitted with glass reservoirs using epoxy resin (Epoxy Technology, Billerica, MA). A Nanoport assembly placed on reservoir 5 (Figure 1B), a microsplitter valve, threaded adapters, and PEEK tubing, all from Upchurch Scientific (Oak Harbor, WA), were used to connect the microfluidic device to the syringe pump.

The cured PDMS was peeled off the mold and placed over the glass slide with the ends of the channels aligned with the access holes on the glass slide. Another glass slide was placed on top, and the excess PDMS was trimmed off. The channel dimensions were determined by measuring the height and width of the features on the silicon wafer mold using a profilometer (Ambios Technology, Santa Cruz, CA). The channels were 19 μm deep, corresponding to the height of the features on the mold. The narrow sections of the channels were 50 μm wide. The wide sections of the channel from reservoirs 1, 2, 3, and 4 were 160 μm, while that from reservoir 5 was 500 μm (Figure 1B).

Cell Culture. Jurkat cells from the Jurkat Clone E6-1 cell line (ATCC TIB-152 American Type Culture Collection, Rockville, MD) were cultured in RPMI 1640 medium containing 10% (v/v) fetal bovine serum, L-glutamine (2 mM), penicillin (100 μg/mL), and streptomycin (100 μg/mL). The cells were maintained in a humidified environment at 37 °C and 5% CO_2 and cultured in 25 mL polystyrene culture flasks (Becton Dickinson Labware, Fisher Scientific). Cells were passaged every 2−3 days.

LPS Stimulation Protocol. NO production in cells was stimulated using purified lipopolysaccharide (LPS) from the *Escheria coli* line 0111:B4 (Sigma Aldrich). An amount of 1.5 μL of 1 mg/mL LPS was administered per milliliter of cell suspension of healthy Jurkat cells and allowed to incubate for 1−3 h. An unstimulated (native) flask of Jurkat cells from the same population was incubated under the same conditions as the control for the stimulation experiment.

Sample Preparation. The cells were labeled with DAF-FM DA, which is fluorogenic and membrane permeable. Once inside the cell, DAF-FM DA is hydrolyzed by nonspecific cytosolic esterases to form 4-amino-5-methylamino-2′,7′-difluorofluorescein (DAF-FM). The hydrolyzed dye further reacts with a partially oxidized species of NO (N_2O_3) to form a triazole (DAF-FM T), which has a high fluorescence yield.[50] We colabeled the cells with 6-CFDA, which is also fluorogenic and membrane permeable and is hydrolyzed by esterases to yield a charged fluorescent moiety that is membrane impermeable. We used 6-CFDA as an internal standard to correct for differences in fluorescence intensity when using different devices. The fluorescence signal of 6-CFDA was not

affected when cells were incubated with LPS. The two dyes were received as lypholyzed powders, and stock solutions were prepared daily for each new set of experiments using 99.9% DMSO. The dye solution was prepared by adding appropriate volumes of the two stock solutions to enough sterile PBS to make a 2 μM DAF-FM DA and 2 μM 6-CFDA solution. An amount of 1 mL of the cell suspension was centrifuged at 2000 rpm (Marathon 8K, Fisher Scientific, Pittsburgh, PA) for 1 min, and the supernatant was discarded. The cells were then resuspended in the dye solution and incubated for 20 min at 37 °C on a heat block. Another centrifugation was performed under the same conditions to remove the dye solution, and the labeled cells were resuspended in RPMI medium containing 2% (w/v) BSA prior to experiments.

Microchip Operation. The separation buffer consisted of 25 mM sodium borate, 20% v/v acetonitrile, 2% w/v BSA, 0.6% w/v Tween-20, and 2 mM SDS. Initially, all the reservoirs were filled with the separation buffer by applying reverse pressure facilitated by a vacuum pump. Reservoir 2 (Figure 1B) was evacuated and replaced with a suspension of the fluorescently labeled cells. The waste reservoir was threaded to provide the connection, via PEEK tubing, to a 1000 μL glass syringe on a syringe pump (New Era Pump Systems, Inc., Farmingdale, NY). Cell transport and fluid flow in the channel manifold were achieved by setting the syringe pump at withdrawal mode at a flow rate of 0.25 μL/min and adjusting the flow splitter until the cells were traveling at a rate at which most of the lysate from the cells was injected into the separation channel.

Cell lysis and subsequent electrophoretic injection and separation were achieved by applying 3 kV using a high voltage supply (Spellman High Voltage Electronics, Hauppauge, NY) across reservoirs 1 and 4 (Figure 1B). (Safety Warning: Appropriate caution should be exercised when working with high voltages.)

Detection. A multiline argon-ion laser (MellesGriot Laser Group, Carlsbad, CA) was used as the excitation source. The 488 nm beam was selected using a dispersive prism and then reflected off a series of mirrors and directed into a Nikon eclipse TS100 microscope (Nikon Instruments, Inc., Melville, NY) through the rear port and via a 20× objective (Plan Fluor, Nikon) to the microscope stage. The beam was focused onto a small spot in the separation channel, 5 mm below the lysis intersection. The fluorescence emission from the dyes was detected by a photomultiplier tube (Hamatsu Instruments, Bridgewater, NJ) attached to the trinocular port of the microscope. (Safety Warning: Appropriate caution should be exercised when working with focused laser light.) The signal was amplified using a low noise current preamplifier at 1 μA/V with 100 Hz low-pass filter (Stanford Research Systems, Sunnyvale, CA) and sampled at 100 Hz using a PC1-6036E I/O card (National Instruments, Austin, TX). The program controlling the high voltage power supply and data acquisition was written in-house using LabVIEW (National Instruments, Austin, TX). Data analysis was performed using Igor Pro (WaveMetrics, Portland, OR).

Video images of the experiment were collected using a digital color video camera (Exwave HAD, Sony Corporation, Park Ridge, NJ) mounted on the side port of a Nikon TE-2000-U inverted microscope (Melville, NY). Frame grabs retrieved in Image J (NIH) were used to calculate the flow rate of the analytes down the separation channel.

■ RESULTS AND DISCUSSION

A wide variety of microchip designs have been reported in the literature for the analysis of single cells. However, there have been only a couple of very recent papers[26,51] in which the contents of more than 30 individual cells have been measured quantitatively by such devices. One possible reason for this is the difficulty in setting up in these chips the reproducible hydrodynamic flows that are necessary for fast cell transport, efficient cell lysis, and lysate injection. Therefore, a major objective of these studies was to develop a microfluidic chip design that was easy to construct and implement and that could be used routinely to analyze hundreds of cells at a rate of at least 10 cells per minute.

The initial experiments employed a previously published design shown in Figure 1A.[24] In this design, cells are loaded into reservoir 3 and flowed through the intersection to waste (reservoir 5).[24] However, we found that reproducible injection of the cell lysate was difficult to realize with this design because of difficulty in precisely controlling the volumetric flow rates in the channel manifold using an external syringe pump. The flow rates on these devices are in the low nL/min range, and the flows from all of the channels at the lysis intersection must be carefully balanced in order to generate reproducible and complete injection of the lysate from the cell into the separation channel. Unpredictable changes in flow resistances over the course of a run due to partial obstructions in the various channels and small changes from device to device in terms of flow resistance make it difficult to reliably adjust the flow. In addition, there is a lag time in terms of when the flow rate is changed on the external pumping device and when this change is seen at the lysis intersection.

To improve the ruggedness and overall operation of the microfluidic device, therefore, we altered the manner in which the cells were transported into the channel intersection of the chip (region marked by black circle in Figure 1B). In the new design, cells are placed in reservoir 2 and are transported to the lysis area of the chip using the hydrodynamic flow generated by a syringe pump in withdrawal mode at reservoir 5. In this configuration, the cells make a 90° turn into the main channel where they encounter a dc electric field sufficient to lyse the cells. The lysate is then electrophoretically injected into the separation channel while the cell debris is hydrodynamically shunted to a waste channel.

Figure 2 shows consecutive image frames grabbed from a video (Supporting Information) demonstrating the lysis of individual Jurkat cells loaded with Oregon Green using this device. The first image, Figure 2A, shows cells approaching the lysis channel. In the second image (Figure 2B), the cells have entered the lysis channel and are lysed by the electric field. In the next two frames (Figure 2C and Figure 2D), the fluorescent lysate is seen traveling into and down the separation channel electrophoretically toward the anode. The velocity of the lysate was 1.44 mm/s. It took less than 33 ms, the length of time between consecutive video frames, to completely lyse the cell. The cell debris was transported into the waste channel more efficiently with this design than in previous designs (see Figure 2E). In addition to the cell transport redesign, the flow rates on this device were more easily controlled by inserting an adjustable flow splitter into the line between the chip and syringe pump (Figure 1B).

A major advantage of this new design is that a dc electric field could be used for cell lysis rather than the high voltage ac
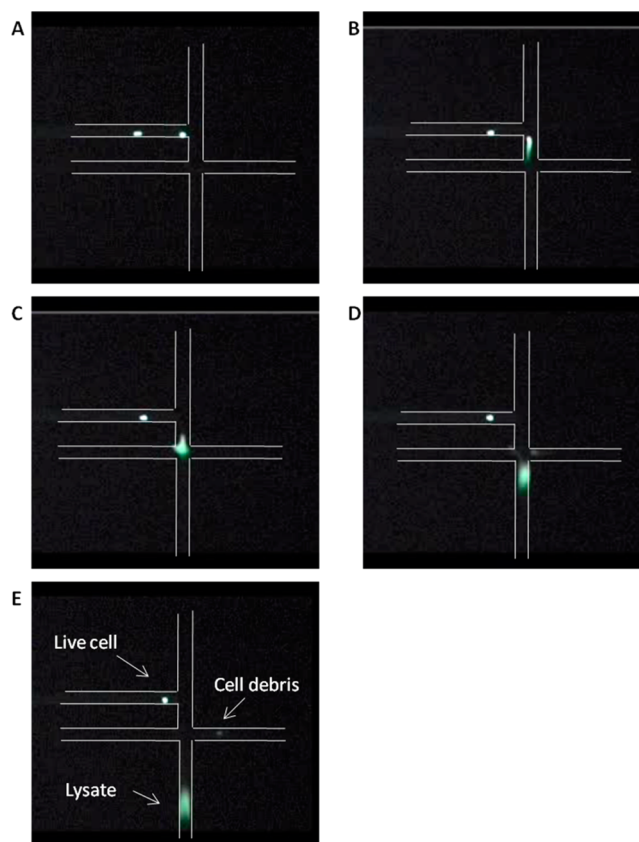

Figure 2. Still images obtained from a video of Jurkat cells lysing. The cells in frame A are hydrodynamically transported toward the lysis intersection. In frame B, the cells at the intersection encounter an electric field that causes them to lyse. In frames C−E, the cell lysate is electrophoretically transported down the separation channel while the cell debris is shunted to the waste channel.

electric field previously reported.[24] This is important, as the high field ac requires a specialized and expensive generator. In addition, the dc electric field strength necessary for consistent cell lysis and lysate injection was less than half that of the previously reported required ac electric field strength.[24] The constant voltage applied between reservoirs 1 and 4 (Figure 1B) generated a field strength of ~375 V/cm in the cell lysing region of the chip.[24] The significantly lower field strength requirements are due to the substantially longer residence time of the cell in the lysis field and the fact that the cell lysate does not need to change migration direction in order to be injected into the separation channel.

The run buffer contained 2% BSA (w/v), which served as a dynamic coating to reduce the adhesion of cell membranes and other biomolecules to the microchip channel surfaces. BSA also substantially reduced the electroosmotic flow in the separation channel. Under these separation conditions, the electrophoretic mobilities of the two negatively charged reporting dyes used for the NO experiments described below were greater than the electroosmotic flow. Therefore, the analytes were detected as they traveled toward the anodic buffer reservoir (reservoir 4 in Figure 1B) following injection into the separation channel.

Lysate Separation Efficiency. When very high throughput analysis of single cells is performed, it is crucial that the electrophoretic separation is fast and that the peaks exhibit high separation efficiencies. Unfortunately with this device design, it was not possible to directly determine the number of

theoretical plates obtained for the analytes of interest in single cells because the cells entered the intersection randomly during any particular run. Instead, the migration velocities of the 6-CFDA and DAF-FM were calculated from videos of the lysate migration under the same separation conditions as those used to obtain single point separations. The calculated migration velocities (e.g., 1.44 mm/s for 6-CFDA) from these videos were used to convert the temporal peak variances measured on the electropherograms to spatial variances so that the peak dispersion could be calculated and compared to predicted values. The predicted (or theoretical) peak dispersion values were calculated based upon the published diffusion coefficient of fluorescein[52] together with the peak broadening expected from the parabolic flow generated in the separation channel from the syringe pump.

The fluidic resistances in the channel manifold were designed so that the overall flow out of the separation channel was only about 3% of the flow going into channel 5 (see Supporting Information S2). The experimentally determined peak dispersion coefficient was 1.1×10^{-5} cm^2/s. The predicted dispersion from diffusion $(4.5 \times 10^{-6}$ cm^2/s)[52] and the hydrodynamic (parabolic) flow (negligible compared to the diffusion) in the separation channel was $\sim 4.5 \times 10^{-6}$ cm^2/s. The experimentally measured value is only ~ 2.5 times that of the predicted value. Given the crude and indirect nature of these measurements, the agreement is remarkably good and shows that the separations are behaving as expected.

Measurement of NO Production in Jurkat Cells. The optimized microfluidic device described above was then used to determine NO production in a population of individual Jurkat cells. The generation of NO by this cell type was measured in bulk previously by our groups using microchip electrophoresis with LIF detection, making direct comparison of the bulk cell measurements with those of single cell distributions possible.[10]

Cells were stimulated with LPS, which is known to up-regulate expression of iNOS, resulting in increased intracellular NO production. Control cells were treated in the same manner but were not exposed to LPS. The intracellular production of NO production in the cells was measured using DAF-FM DA. The cells were colabeled with 6-CFDA, which was used as an internal standard to account for variation in fluorescence intensity when using different microchips and for differences in cell size (volume) as well as variations in esterase activity. The fluorescence yield of 6-CFDA was not affected by the presence of intracellular NO.

The analytes present in the cell lysates were detected using laser-induced fluorescence at a distance of 5 mm from the intersection on the separation channel. Figure 3 shows typical electropherograms obtained for native and stimulated cells. Three distinct peaks are observed. The first tall peak indicates partially hydrolyzed 6-CFDA (6-CFp). The second peak is the completely hydrolyzed 6-CFDA (6-CF). The last peak is the benzotriole derivative of DAF-FM (DAF-FM T) that corresponds to the NO concentration in the cell. The peak identities were verified by labeling a separate batch of cells with the individual dyes (Supporting Information S3).

The device was then used for the analysis of populations of control and stimulated cells. Because of the lack of a "cell standard," it was not possible to directly quantitate the amount of NO produced in these experiments. However, the ratio of DAF-FM to the products of the 6-CF hydrolysis could be used to evaluate the relative change in NO production in basal versus stimulated cells. Table 1 shows the DAF-FM T, 6-CF, and 6-
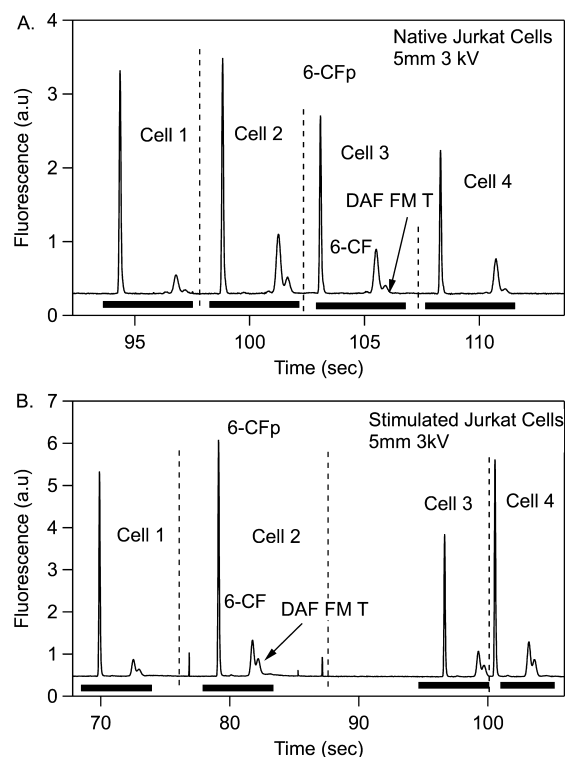

Figure 3. Electrophoretic separation of dyes released from individual cells. These are 20 and 30 s segments from a 120 s run. Each cell produced a peak envelope consisting of one tall peak due to partially hydrolyzed 6-CFDA (6-CFp) and a shorter doublet ~ 3 s later due to fully hydrolyzed 6-CFDA (6-CF) and DAF-FM T. There is a marked increase in DAF-FM T peak height relative to the 6-CF peak following stimulation.

CFp peak height and peak area ratios. As can be seen from this table, the ratio of the two products of 6-CF does not change upon stimulation, but the ratio of DAF-FM T to either of these "internal standards" doubles (Table 1).

Figure 3B shows a representative electropherogram obtained for the Jurkat cells after 3 h of stimulation. The addition of LPS resulted in an increase in NO production as shown by the relative increase in the DAF-FM T peak compared to the 6-CF and 6-CFp peaks in Figure 3B versus the control cells in Figure 3A. A histogram of the distributions of the DAF-FM T/6-CF ratios for 100 stimulated versus 100 control cells is shown in Figure 4. The other distributions are available in the Supporting Information S4. The relative increase in NO production for the stimulated cells was calculated using eq 1 below.

$$\left(\frac{\left[\frac{\text{DAF-FM T}}{\text{6-CFDA}} \right]_{\text{stimulated}} - \left[\frac{\text{DAF-FM T}}{\text{6-CFDA}} \right]_{\text{native}}}{\left[\frac{\text{DAF-FM T}}{\text{6-CFDA}} \right]_{\text{native}}} \right) \times 100 \tag{1}$$

Both the peak height and peak area ratios indicate a 2-fold increase in NO concentration following 3 h stimulation of cells with LPS (Table 1). A comparison-of-the-means-of-two-independent-samples t-test between the relative NO concentrations in the native and stimulated cells shows the difference to be statistically significant for both the peak height and peak area ratios ($n = 199$; $p < 0.0005$).[53]

There are a variety of potential interferences that can arise when using DAF-FM DA as a probe molecule for NO. For example, DAF FM can produce a fluorescent species because of

Table 1. Average Peak Ratios[a]

peak area ratio	6-CF/6-CFp	DAF-FM T/6-CF	DAF-FM T/6-CFp	no. of cells
native cells	0.46 ± 0.26	0.39 ± 0.34	0.16 ± 0.12	100
stimulated cells	0.48 ± 0.15	0.72 ± 0.21	0.34 ± 0.12	100
mean stimulated/mean native ratio	1.00 ± 0.30	1.80 ± 0.40	2.10 ± 0.17	
peak height ratio	6-CF/6-CFp	DAF-FM T/6-CF	DAF-FM T/6-CFp	no. of cells
native cells	0.21 ± 0.31	0.26 ± 0.08	0.054 ± 0.07	100
stimulated cells	0.17 ± 0.05	0.61 ± 0.13	0.10 ± 0.03	100
mean stimulated/mean native ratio	0.80 ± 0.31	2.30 ± 0.15	1.90 ± 0.08	

[a]The upper portion of the table contains the average peak area ratios, while the lower portion of the table contains the average peak height ratios. The standard deviations for each measurement are reported.
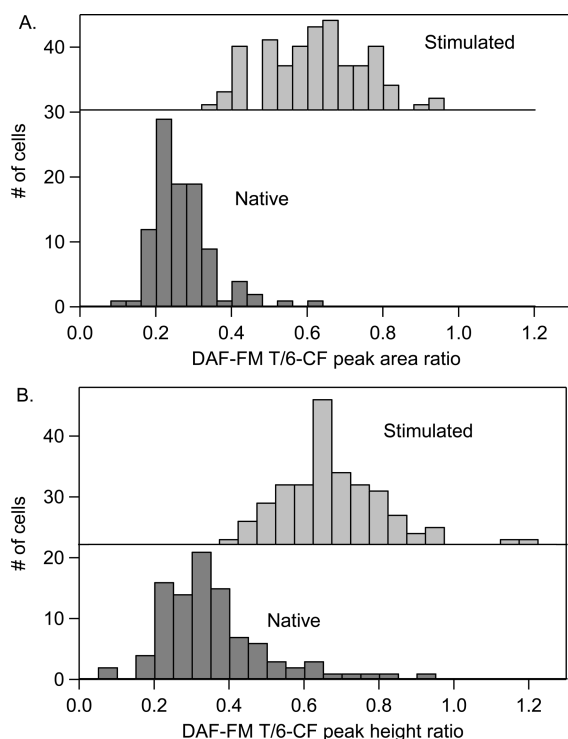

Figure 4. (A) Histogram of DAF-FM T/6-CF peak area ratios calculated for 100 native cells (dark gray) and stimulated cells (light gray) and (B) histogram of peak height ratios of the same cells. The peak ratios of cells increase because of increased NO production following stimulation of Jurkat cells with LPS for 3 h.

photo-oxidation of the probe, contamination of DAF FM T, or formation of interfering products due to dehydroascorbic acid.[54,55] Also, DAF FM can produce fluorescent species by superoxide. However, DAF FM does not produce interfering products due to peroxynitrite (low concentrations, below 10 μM), nitrite, and H_2O_2, although H_2O_2 can enhance the fluorescence of DAF FM when NO is present.[54] These issues were addressed in our bulk cell studies paper that was previously published in *Analytical Methods*.[10] In that study we showed the separation of DAF FM DHA (the fluorescent product due to dehydroascorbic acid) from DAF FM T and that only a negligible peak due to DAF FM DHA was observed.[10] Under the present separation conditions, DAF FM and DAF FM T comigrate; however, we observed negligible fluorescence from DAF FM itself.[10] Additionally, Hoegger's group has shown that DAF FM can form fluorescence products during DAF FM freeze–thaw cycles.[10] To prevent these issues, we prepared new DAF FM DA stock solutions for each set of experiments.

Device Ruggedness. All of the data shown in Figure 4 were obtained from cells using the same device over the course of 14 sequential runs: 7 for the native cells and 7 for the stimulated cells. At least 20 cells were detected for each run, but 20 cells were not always analyzed because of peak overlap. The results for the video analysis and the diffusion coefficient measurements were obtained using separate devices. We did not perform quantitative device-to-device comparisons in these studies. However, in all cases, a single device could be used multiple times before failing.

Bulk vs Single Cell Analysis. We recently published a report on the NO concentration levels in native and stimulated Jurkat bulk cell lysates using microchip electrophoresis with LIF detection.[10] The stimulation and measurement parameters used in these studies were carried out as close as possible to those used in the previous paper. This makes it possible to compare these single cell analysis results with those obtained previously via bulk cell measurements. The average DAF-FM T/6-CFDA peak height ratios are 2.3 ± 0.15 times greater for the stimulated cells compared to the native cells. The average single cell results are in remarkably close agreement (2-fold increase) to the bulk cell analysis results, which showed a 2.2 ± 0.2 increase upon LPS stimulation. In addition, reports with other cells types show a similar increase in NO production upon stimulation by LPS only.[10,14,56,57]

In our previous paper the average amount of NO produced per cell was quantitated using a true NO standard with the average native cell producing 0.6 ± 0.1 mM NO and a stimulated cell producing 1.5 ± 0.4 mM NO.[10] Given the similar conditions under which the experiments were performed and the similar increase seen in the DAF-FM T/6-CF peak height and area ratios, it is probable that the average amount of NO in the cells is comparable to these previous results.

One limitation with the device as it is now configured is that the injection voltage is continuously on, so that whenever a cell enters the lysis intersection, it is automatically injected. This makes it difficult to generate calibration curves to make quantitative measurements, as gated injections cannot easily be generated. This calibration issue, however, can potentially be overcome through the packaging of calibration standards in liposomes.

■ CONCLUSIONS

We have developed an integrated glass–PDMS hybrid microfluidic device for high throughput analysis of single cells. The device uses a new channel manifold design to significantly improve the reliability and robustness of the cell lysis and lysate injection. Intracellular detection of NO in single cells was accomplished using DAF-FM (a NO-specific

fluorophore) and 6-CFDA (an internal standard). The single cell analysis system was used to determine the increase in NO production following stimulation with LPS. A 3 h stimulation of the cells with LPS resulted in a 2-fold increase in NO production. A comparison of bulk and single cell NO measurements was performed, and the average NO production in single cells compared well to the increase measured at the bulk cell level. In future studies, we will incorporate electrodes in the bulk and single cell analysis chips for the simultaneous detection of NO, peroxynitrite, and other molecules that play an important role in inflammation, including glutathione, ascorbic acid, and nitrotyrosine, by microchip electrophoresis with amperometric detection.

■ ASSOCIATED CONTENT

Ⓢ Supporting Information

Video mpg file of cell lysis and pdf file containing fluidic resistance calculation, determination of separation efficiencies, electropherograms of cells labeled with 6-CFDA, and histograms for comparison of stimulated and native cells. This material is available free of charge via the Internet at http://pubs.acs.org.

■ AUTHOR INFORMATION

Corresponding Author

*E-mail: culbert@ksu.edu. Phone: +1-785-532-6685. Fax: +1-785-532-6666.

Notes

The authors declare no competing financial interest.

■ ACKNOWLEDGMENTS

■ REFERENCES

(1) Brehm-Stecher, B. F.; Johnson, E. A. *Microbiol. Mol. Biol. Rev.* **2004**, *68*, 538−559.
(2) Wang, D.; Bodovitz, S. *Trends Biotechnol.* **2010**, *28*, 281−290.
(3) Varin, A.; Gordon, S. *Immunobiology* **2009**, *214*, 630−641.
(4) Gordon, S. *Nat. Rev. Immunol.* **2003**, *3*, 23−35.
(5) Brombacher, F.; Arendse, B.; Peterson, R.; Hoelscher, A.; Hoelscher, C. *Methods Mol. Biol. (Totowa, NJ, U. S.)* **2009**, *531*, 225−252.
(6) Tymvios, C.; Moore, C.; Jones, S.; Solomon, A.; Sanz-Rosa, D.; Emerson, M. *Br. J. Pharmacol.* **2009**, *158*, 1735−1742.
(7) Tiscornia, A.; Cairoli, E.; Marquez, M.; Denicola, A.; Pritsch, O.; Cayota, A. *J. Immunol. Methods* **2009**, *342*, 49−57.
(8) Yasuda, H. *Nitric Oxide* **2008**, *19*, 205−216.
(9) Muller, G.; Morawietz, H. *Antioxid. Redox Signaling* **2009**, *11*, 1711−1731.
(10) Mainz, E. R.; Gunasekara, D. B.; Caruso, G.; Jensen, D. T.; Hulvey, M. K.; Fracassi, d. S. J. A.; Metto, E. C.; Culbertson, A. H.; Culbertson, C. T.; Lunte, S. M. *Anal. Methods* **2012**, *4*, 414−420.
(11) Floyd, P. D.; Moroz, L. L.; Gillette, R.; Sweedler, J. V. *Anal. Chem.* **1998**, *70*, 2243−2247.
(12) Ye, X.; Xie, F.; Romanova, E. V.; Rubakhin, S. S.; Sweedler, J. V. *ACS Chem. Neurosci.* **2010**, *1*, 182−193.
(13) Ye, X.; Kim, W.-S.; Rubakhin, S. S.; Sweedler, J. V. *J. Neurochem.* **2007**, *101*, 632−640.
(14) Kim, W.-S.; Ye, X.; Rubakhin, S. S.; Sweedler, J. V. *Anal. Chem.* **2006**, *78*, 1859−1865.
(15) Cruz, L.; Moroz, L. L.; Gillette, R.; Sweedler, J. V. *J. Neurochem.* **1997**, *69*, 110−115.
(16) Moroz, L. L.; Dahlgren, R. L.; Boudko, D.; Sweedler, J. V.; Lovell, P. *J. Inorg. Biochem.* **2005**, *99*, 929−939.
(17) Vogel, P. A.; Halpin, S. T.; Martin, R. S.; Spence, D. M. *Anal. Chem.* **2011**, *83*, 4296−4301.
(18) Halpin, S. T.; Spence, D. M. *Anal. Chem.* **2010**, *82*, 7492−7497.
(19) Letourneau, S.; Hernandez, L.; Faris, A. N.; Spence, D. M. *Anal. Bioanal. Chem.* **2010**, *397*, 3369−3375.
(20) Spence, D. M.; Torrence, N. J.; Kovarik, M. L.; Martin, R. S. *Analyst* **2004**, *129*, 995−1000.
(21) Wilson, H. M. *J. Cell. Mol. Med.* **2010**, *14*, 2055−2065.
(22) Mantovani, A.; Garlanda, C.; Locati, M. *Arterioscler., Thromb., Vasc. Biol.* **2009**, *29*, 1419−1423.
(23) Colton, C. A. *J. Neuroimmune Pharmacol.* **2009**, *4*, 399−418.
(24) McClain, M. A.; Culbertson, C. T.; Jacobson, S. C.; Allbritton, N. L.; Sims, C. E.; Ramsey, J. M. *Anal. Chem.* **2003**, *75*, 5646−5655.
(25) Lin, Y.; Trouillon, R.; Safina, G.; Ewing, A. G. *Anal. Chem.* **2011**, *83*, 4369−4392.
(26) Phillips, K. S.; Lai, H. H.; Johnson, E.; Sims, C. E.; Allbritton, N. L. *Lab Chip* **2011**, *11*, 1333−1341.
(27) Liu, Y.-M.; Zhao, S.; Alterman, M. A.; Hunziker, P. In *Amino Acid Analysis: Methods and Protocols*; Walker, J. M., Ed.; Humana Press: New York, 2012; p 351.
(28) Hosokawa, M.; Hayashi, T.; Mori, T.; Yoshino, T.; Nakasono, S.; Matsunaga, T. *Anal. Chem.* **2011**, *83*, 3648−3654.
(29) Jiang, D.; Sims, C. E.; Allbritton, N. L. *Electrophoresis* **2010**, *31*, 2558−2565.
(30) Lai, H. H.; Quinto-Su, P. A.; Sims, C. E.; Bachman, M.; Li, G. P.; Venugopalan, V.; Allbritton, N. L. *J. R. Soc. Interface* **2008**, *5* (Suppl. 2), S113−S121.
(31) Trouillon, R.; Passarelli, M. K.; Wang, J.; Kurczy, M. E.; Ewing, A. G. *Anal. Chem.* **2013**, *85*, 522−542.
(32) Kovarik, M. L.; Gach, P. C.; Ornoff, D. M.; Wang, Y.; Balowski, J.; Farrag, L.; Allbritton, N. L. *Anal. Chem.* **2012**, *84*, 516−540.
(33) Price, A. K.; Culbertson, C. T. *Anal. Chem.* **2007**, *79*, 2614−2621.
(34) Dickinson, A. J.; Armistead, P. M.; Allbritton, N. L. *Anal. Chem.* **2013**, *85*, 4797−4804.
(35) Cecala, C.; Rubakhin, S. S.; Mitchell, J. W.; Gillette, M. U.; Sweedler, J. V. *Analyst* **2012**, *137*, 2965−2972.
(36) Culbertson, C. T. In *Microchip Capillary Electrophoresis*; Henry, C., Ed.; Humana: Totowa, NJ, 2006; pp 203−216.
(37) Cecala, C.; Sweedler, J. V. *Analyst* **2012**, *137*, 2922−2929.
(38) Sims, C. E.; Allbritton, N. L. *Lab Chip* **2007**, *7*, 423−440.
(39) Lion, N.; Reymond, F.; Girault, H. H.; Rossier, J. S. *Curr. Opin. Biotechnol.* **2004**, *15*, 31−37.
(40) Roman, G. T.; Chen, Y. L.; Viberg, P.; Culbertson, A. H.; Culbertson, C. T. *Anal. Bioanal. Chem.* **2007**, *387*, 9−12.
(41) Yin, H.; Marshall, D. *Curr. Opin. Biotechnol.* **2012**, *23*, 110−119.
(42) Kovarik, M. L.; Shah, P. K.; Armistead, P. M.; Allbritton, N. L. *Anal. Chem.* **2013**, *85*, 451−472.
(43) Greif, D.; Galla, L.; Ros, A.; Anselmetti, D. *J. Chromatogr., A* **2008**, *1206*, 83−88.
(44) Xu, C.-X.; Yin, X.-F. *J. Chromatogr., A* **2011**, *1218*, 726−732.
(45) Zhu, L.; Lu, M.; Yin, X. *Talanta* **2008**, *75*, 1227−1233.
(46) Zhang, X.; Li, Q.; Chen, Z.-z.; Li, H.; Xu, K.; Zhang, L.; Tang, B. *Lab Chip* **2011**, *11*, 1144−1150.
(47) Yu, L.; Huang, H.; Dong, X.; Wu, D.; Qin, J.; Lin, B. *Electrophoresis* **2008**, *29*, 5055−5060.
(48) Hargis, A. D.; Alarie, J. P.; Ramsey, J. M. *Electrophoresis* **2011**, *32*, 3172−3179.
(49) Duffy, D. C.; McDonald, J. C.; Schueller, O. J. A.; Whitesides, G. M. *Anal. Chem.* **1998**, *70*, 4974−4984.

(50) Yang, Q.; Zhang, X.; Bao, X.; Lu, H.; Zhang, W.; Wu, W.; Miao, H.; Jiao, B. *J. Chromatogr., A* **2008**, *1201*, 120−127.

(51) Shah, D.; Steffen, M.; Lilge, L. *Biomicrofluidics* **2012**, *6*, 014111−014121.

(52) Culbertson, C. T.; Jacobson, S. C.; Ramsey, J. M. *Talanta* **2002**, *56*, 365−373.

(53) Marssart, D. L.; Vandeginste, B. G. M.; Deming, S. N.; Michotte, Y.; Kaufman, L. *Chemometrics: A Textbook*; Elsevier: Amsterdam, 1988; Vol. 2, p 488.

(54) Balcerczyk, A.; Soszynski, M.; Bartosz, G. *Free Radical Biol. Med.* **2005**, *39*, 327−335.

(55) Zhang, X.; Kim, W.-S.; Hatcher, N.; Potgieter, K.; Moroz, L. L.; Gillette, R.; Sweedler, J. V. *J. Biol. Chem.* **2002**, *277*, 48472−48478.

(56) Koide, N.; Sugiyama, T.; Mori, I.; Mu, M. M.; Yoshida, T.; Yokochi, T. *J. Endotoxin Res.* **2003**, *9*, 85−90.

(57) Goto, M.; Sato, K.; Murakami, A.; Tokeshi, M.; Kitamori, T. *Anal. Chem.* **2005**, *77*, 2125−2131.